Quantitative Local Photosynthetic Flux Measurements at Isolated Chloroplasts and Thylakoid Membranes using Scanning Electrochemical Microscopy (SECM)

Kim McKelvey[a,b,c], *Sophie Martin*[a], *Colin Robinson*[c] *and Patrick R. Unwin*[a]*

[a]Department of Chemistry, [b]Molecular Assembly and Organisation in Cells (MOAC) Doctoral Training Centre and [c]School of Life Sciences, University of Warwick, Coventry, U.K. CV4 7AL

*Department of Chemistry, University of Warwick, Coventry, U.K. CV4 7AL. +44 (0)2476 523264. P.R.Unwin@warwick.ac.uk

Abstract

Scanning electrochemical microscopy (SECM) offers a fast and quantitative method to measure local fluxes within photosynthesis. In particular, we have measured the flux of oxygen and ferrocyanide ($Fe(CN)_6^{4-}$), from the artificial electron acceptor ferricyanide ($Fe(CN)_6^{3-}$), using a stationary ultramicroelectrode at chloroplasts and thylakoid membranes (sourced from chloroplasts). Oxygen generation at films of chloroplasts and thylakoid membranes was detected directly during photosynthesis, but in the case of thylakoid membranes this switched to sustained oxygen consumption at longer illumination times. An initial oxygen concentration spike was detected over both chloroplast and thylakoid membrane films, and the kinetics of the oxygen generation were extracted by fitting the experimental data to a finite element method (FEM) simulation. In contrast to previous work, the oxygen generation spike was attributed to the limited size of the plastoquinone pool, a key component in the linear electron transport pathway and a contributing factor in photoinhibition. Finally, the mobile nature of the SECM probe, and its high spatial resolution, also allowed us to detect ferrocyanide produced from a single thylakoid membrane. These results further demonstrate the power of SECM for localized flux measurements in biological processes, in this case photosynthesis, and, that the high time resolution, combined with FEM simulations, allows the elucidation of quantitative kinetic information.

Keywords : Oxygen, Kinetics, Photosynthesis, Plastoquinone, Bioelectrochemistry.

Introduction

Photosynthesis is the ultimate source of virtually all metabolic energy, converting sunlight to a useable form of chemical energy to drive otherwise endogenic reactions needed for the growth and maintenance of organisms.[1,2] Within higher plants, all the primary processes of photosynthesis, e.g. light capture and electron transport, leading to NADPH and ATP synthesis, and many secondary processes,[1,2] are located in the chloroplast. The light-dependent components of the photosynthetic pathway are embedded in the thylakoid membrane, which is contained within the chloroplast, as illustrated schematically in Figure 1 A. Isolated chloroplasts and thylakoid membranes have consequently been used extensively to investigate aspects of photosynthesis,[2] but the majority of investigations have been performed on large populations, with data averaged over many individual chloroplasts or thylakoid membranes. This averaging reduces the temporal resolution of any measurement and, as such, obscures potentially interesting kinetic aspects of photosynthesis.

Microscopy investigations of individual chloroplasts and thylakoid membranes have tended to focus on structure, rather than the flux of chemical species, using techniques such as optical microscopy,[3–5] electron microscopy,[6–8] atomic force microscopy,[9,10] or scanning tunneling microscopy.[11] Optical microscopy techniques, such as fluorescence microscopy, provide some opportunities to access chemical fluxes from individual cells (or components) but this is indirect, requiring the use of appropriate indicators.[12,13]

In terms of flux measurements, scanning electrochemical microscopy (SECM) is particularly suited to detect a wide range of redox-active species with high spatial and temporal resolution.[14–18] A small electrode (tip) is immersed in solution close to a sample and the current response at the electrode, arising from electrochemical processes taking place at the electrode, is recorded. A

diagram of a typical SECM tip investigating a redox process ($Fe(CN)_6^{4-/3-}$) at a surface is shown in Figure 1 B. The spatial resolution of SECM is governed by the size of the electrode, which is typically in the region of 100 nm - 25 μm,[14] and the distance of the tip from the surface.[19] The geometry of the SECM tip, and the ability to place it at a defined distance from a sample, allows the flux of the redox-active species at the sample to be calculated from the current measured, by solving the underlying mass transport problem.[20–22]

SECM is proving increasingly popular for studying living cell monolayers and individual cells.[23–34] Particularly relevant to this study are previous reports on aspects of photosynthesis,[35,36] for example, measurements of the local oxygen flux from single stomata of *Brassica juncea*[37] and the local oxygen flux above individual guard cells in intact plant leaves.[38] Two-dimensional imaging of the oxygen evolution from a single protoplast[39] (a plant cell with the cell wall removed) and quantification of the steady-state oxygen generation from single protoplasts[40–42] have also been reported. An individual component of the light-dependent photosynthetic pathway, photosystem I, has been investigated electrochemically[43] and using SECM.[44] In addition, the insertion of an AFM tip with an integrated electrode into single algal cells and chloroplasts has also been recently demonstrated, with the direct extraction of electrons from the photosynthetic pathway and oxygen evolution in the cytosolic space reported.[45–47] These studies have tended to provide measurements of steady-state oxygen generation rates, but have not exploited the ability of SECM to investigate processes with exquisite time resolution, an aspect we demonstrate to be particularly powerful for the studies herein.

The fragile nature of individual chloroplasts makes them prone to lysis, and so it is important to establish the state of the chloroplasts within the experimental configuration. Oxygen evolution in the presence of ferricyanide is a well established method for measuring the proportion of burst chloroplasts in an ensemble in suspension.[48–51] Ferricyanide is a well-known anionic, non-

physiological electron acceptor (producing ferrocyanide) which can only freely interact with thylakoid membranes upon bursting of the chloroplast envelope.[52] Once through the chloroplast envelope, the impermeability of the thylakoid membrane only allows the ferricyanide/ferrocyanide redox couple to act on the stromal side of photosystem II (PSII).[53–55] This reaction involves the light-driven transfer of electrons from water to the ferricyanide/ferrocyanide couple, with concomitant evolution of oxygen. In this way, envelope intactness can be determined by measuring the flux of ferrocyanide generated under illumination.

The goals of this paper were several-fold: first, to use SECM methodology to assess whether isolated chloroplasts (and, by extension, thylakoid membranes) films are a viable configuration in which to study photosynthesis. Such a configuration opens up the possibility of high resolution measurements of individual chloroplasts and thylakoid membranes. This was carried out by assaying the intactness of a chloroplast film by the electrochemical detection of ferrocyanide before and after osmotically shocking the film to burst all of the organelles. Second, we determine the oxygen evolution and consumption at isolated, immobilized chloroplast and thylakoid membrane films during photosynthesis by the direct detection of the oxygen. The temporal resolution of SECM allows local oxygen generation and consumption rates to be measured on much shorter timescales than previously. Kinetic data were extracted, analyzed and interpreted by developing a finite element method (FEM) simulation, which faithfully represents the physicochemical processes and mimics the geometry of the SECM configuration. In addition, the effect of Mg^{2+}, Mn^{2+} and Cl^{-}, which are thought to play a role in photosynthesis,[56–59] was assessed at chloroplast films. Finally, and with an eye to the future, we demonstrate the use of SECM to determine the turnover rate of the ferricyanide/ferrocyanide redox couple on a single thylakoid membrane.

Experimental

Instrumentation

An SECM mounted either on a confocal/fluorescence microscope (TCS SP5 MP, Leica) or an inverted microscope (Axiovert 25, Zeiss) was used for these studies. The tip electrode was positioned using micropositioners (Newport Corp) for coarse control and piezoelectric positioners, either a Nanocube P-611.3S (Physik Instrumente) or Trito 100 (Piezosystems Jena), for fine control. A two-electrode setup was used for dynamic electrochemical measurements, with the current measured using either a home-built current follower through a FPGA card (PCIe-7852R, National Instruments) controlled using LabVIEW software (LabVIEW 2011, National Instruments) interface or a potentiostat (CH730A, CH Instruments). The working electrode (SECM tip) was typically a 25 μm diameter Pt or Ag disk-ultramicroelectrode (UME), and a AgCl-coated Ag wire was used as a quasi-reference counter electrode (QRCE), against which all potentials are quoted. The sample was illuminated by either the fluorescence microscope, with an I3 filter set (band pass filter 470 ± 20 nm and dichroic mirror 510 nm, Leica), or a halogen lamp (HL-2000-HP-232, Ocean Optics), with a 650 ± 80 nm bandpass filter, which was controlled via a personal computer (Faulhaber motion manager 2). The light intensity was measured using a silicon detector photodiode (NT 53-375, Edmund Industrial Optics).

Confocal laser scanning microscopy (CLSM) of individual chloroplasts and thylakoid membranes was obtained with a Zeiss LSM 510 microscope, using a water immersion objective lens (Zeiss, Achroplan 63 x / 0.95 W) with an argon laser (λ = 488 nm) and 505 nm long pass filter.

Materials and Chemicals

Solutions: A series of buffer solutions was used, as defined in Table 1, with all chemicals of the highest grade from Sigma-Aldrich. Solutions were prepared with Milli-Q reagent grade water (resistivity of ca. 18.2 MΩ cm at 25°C). Percoll pads (2 ml of 5×HS buffer, 3.5 ml Percoll (Sigma-Aldrich), 4.5 ml H_2O) were used in the preparation of the chloroplasts. Poly-L-lysine (PLL) (Sigma-Aldrich) was used to prepare the slide surfaces onto which chloroplasts and thylakoid membranes were immobilized. Ferricyanide ($Fe(CN)_6^{3-}$, Fischer Chemicals) as the potassium salt was used as purchased.

Samples: Chloroplasts were isolated from 8 to 9 day old peas (*Pisum sativum*, var. Kelvedon Wonder) by the mechanical disruption method.[60] In brief, leaves were homogenized using a Polytron blender (Kinematica GmbH) in HEPES-Sorbitol (HS) buffer (defined in Table 1), before being filtered through a double layer of Microcloth (Calbiochem) and centrifuged at 3300 g for 2 minutes. The chloroplast pellet was re-suspended in 2 ml of HS buffer and transferred onto a Percoll pad, centrifuged at 1400 g for 8 minutes and the supernatant discarded. The pellet was resuspended in 10 ml HS buffer, centrifuged at 3000 g for 2 minutes before finally being re-suspended in a minimum volume (0.5 - 0.8 ml) of HS buffer. The chlorophyll content was determined spectrophotometrically using the method of Arnon[61] and adjusted to 2.0 mg/ml. Thylakoid membranes were extracted by taking 0.4 ml of chloroplast solution, centrifuged at 7000 rpm for 2 minutes and re-suspending in HEPES-magnesium (HM) buffer (defined in Table 1) for 5 minutes on ice to osmotically lyse the organelles. The lysed chloroplasts were washed twice in HS buffer and once in HM buffer by centrifuging at 14,000 rpm for 2 minutes. The thylakoid membranes were finally re-suspended in 0.4 ml HM buffer at a concentration of 2 mg/ml chlorophyll.

Deposition: Chloroplasts and thylakoid membranes were immobilized onto PLL covered slides, which were prepared by sonicating in acetone and then water for 10 minutes, followed by

drying with nitrogen and immersion in 0.1% (w/v) PLL solution for 5 minutes, and finally curing for 1 hour at 60 °C. 10 µl of either the chloroplast suspension or thylakoid membrane suspension was deposited onto each slide. After two to three minutes for the films and 30 seconds for the individual isolated thylakoid membranes, the slide was gently rinsed twice with the appropriate buffer. The films were relatively uniform and of high coverage, as shown by the optical microscope images (taken on the Leica inverted microscope) shown in Figure 2 A and B. Analysis of the optical images allowed the surface coverage to be determined as *ca.* 3.5×10^6 chloroplasts/cm^2 or 2.5×10^6 thylakoid membranes/cm^2. To further confirm the deposition of the chloroplast and thylakoid membrane films, CLSM z-stacks of individual chloroplasts and thylakoid membranes, shown in Figure 2 A and 2B respectively, were obtained using the intrinsic fluorescence of chlorophyll. These confirmed the height dimensions expected of individual chloroplasts (4 – 5 µm) and thylakoid membranes (2.5 – 3.5 µm), and showed clearly that immobilization results in the formation of a monolayer.

SECM Methods

All measurements were made in solutions which had been pre-chilled with temperatures between 4 and 6 ºC measured during experiments. Pt electrodes are optimal for the detection of ferrocyanide.[33,62] Although Pt could also be used to detect O_2, Ag electrodes have been found to give a more stable response.[63] Prior to measurements, the electrochemical cell was typically equilibrated in the dark for 5 to 10 minutes and the Pt working electrode tips were pre-oxidized at 1.2 for 10 seconds to activate them prior to measurements, while Ag UMEs were used without further pretreatment (after polishing with fine alumina powder).[64] The SECM tips were typically positioned at a distance of 12.5 µm (which corresponded to one electrode radius) above the

sample by using the diffusion-controlled reduction of oxygen or ferricyanide (negative feedback control) for distance control.[22,65]

Chloroplast Intactness: The 25 μm diameter Pt disk UME was used to detect the production of ferrocyanide, before and after osmotically shocking chloroplast films, during illumination (650 nm, flux of 9.4 $x10^{14}$ photons cm^{-2} s^{-1}). The process of osmotically shocking the chloroplasts, adapted from that of Lilley *et al*.,[66] involved soaking the film of immobilized chloroplasts in a solution containing only 10 mM $MgCl_2$ for 1 minute, followed by the addition of double strength HS+ buffer (see Table 1). This was then replaced by HS buffer containing 1 mM ferricyanide as the redox mediator.

Oxygen Evolution/Consumption: The rate of oxygen evolution or consumption by immobilized chloroplast films, in HS and HS+ buffers, and thylakoid membrane films in HM buffer was monitored with an Ag disk UME with an SECM system mounted on an inverted microscope (*vida supra*). The electrode was used to monitor the local oxygen flux as the films of chloroplasts, or thylakoid membranes, were illuminated at four different light fluxes (16%, 26%, 60%, and 100% of maximum defined above). The current-time transient responses for oxygen reduction at the electrode are presented as current magnitude relative to the background response for oxygen reduction at the electrode in the dark (measured accurately before and after illumination as 4.0 ± 0.3 nA). Thus, positive values of the current difference, $I_{Light} - I_{Dark}$, indicate oxygen generation under illumination, whereas negative values indicate oxygen consumption.

Single Thylakoid Membrane Studies: A Pt disk UME was positioned above an individual isolated thylakoid membrane using the fluorescence microscope to aid lateral positioning. The tip was held at a potential for the diffusion-limited oxidation of ferrocyanide to ferricyanide, measured as a function of time, as the sample was illuminated (at 470 nm) at high light intensity

(3.2×10^{16} photons cm^{-2} s^{-1}) through the fluorescence microscope, so as to saturate the photosynthetic pathway. Experiments were carried out with and without 3.3 mM ferricyanide present. Note that the single thylakoid membrane sample was illuminated using a different wavelength of light than for the films, so as to maximize photochemical efficiency. A typical optical image of an UME positioned over a single thylakoid membrane is presented in Figure 2 C, to illustrate the precision in lateral positioning that can be achieved.

Theory and Simulations

Oxygen is generated, as part of the photosynthetic electron transport pathway, from water splitting at the stromal side of photosystem II (PSII). The primary electron acceptor at PSII is plastoquinone (PQ), which accepts electrons (and protons) and diffuses within the thylakoid membrane to donate the electrons to cytochrome b_6f and protons to the thylakoid lumen. The oxidized PQ must then diffuse back to PSII in order to accept further electrons in the chain. However, there is a limited number of PQ molecules present, and under conditions where more energy is absorbed, producing a higher flux of electrons than can be translated, the pool of PQ becomes reduced and acts to block electron transfer.[1,2,67,68] This, in turn, causes photoinhibition, which is the regulation and inactivation of PSII and its associated proteins.[67–70] Therefore, at the reasonably short time periods, which we probe herein, oxygen production largely depends on the overall oxidation state of the PQ pool.[71–74]

Oxygen Generation at Chloroplast Films: We develop FEM simulations based on a kinetic model in which the rate of oxygen generation at the chloroplast film depends on the concentration of oxidized PQ species (N_t) which are consumed (kinetic constant k_f) to produce a reduced PQ species (R_s), but are also regenerated (kinetic constant k_b) to produce the oxidized species.

$$N_t \underset{k_b}{\overset{k_f}{\rightleftarrows}} R_s \quad (1)$$

Therefore, the number of oxidized PQ species, N_t, at time t, where t is the time after switching on the illumination, is:

$$\frac{\partial N_t}{\partial t} = -k_f N_t + k_b (N_0 - N_t) \quad (2)$$

where N_0 is the total number of PQ species, which were all initially in the oxidized state. The above equation can be integrated to give the number of PQ species at time t, from which the flux of oxygen at the chloroplast film (boundary 3 in Figure 3), J, is:

$$J = \frac{k_f N_0 (k_b + k_f e^{-(k_b + k_f)t})}{k_b + k_f} \quad (3)$$

Oxygen Generation at Thylakoid Membrane Films: Thylakoid membranes lack many of the stabilizing components of the photosynthetic pathway, and so the initial oxygen generation, before any limiting factors set in, was investigated and simulated. By focusing on the shortest times, the oxygen flux on the film boundary is set directly.

FEM Simulations: FEM simulations were developed using Comsol Multiphysics 4.3 (Comsol AB) on a 64 bit personal computer. The mass transport of oxygen within the SECM axisymmetric cylindrical configuration is confined to diffusion-only transport, and, as such, is described by Fick's second law:

$$\frac{\partial c}{\partial t} = D\nabla^2 c \quad (4)$$

where c is the concentration of oxygen, and D is the diffusion coefficient of oxygen at 5°C, which is 0.91×10^{-5} cm^2 s^{-1}.[75] The tip-current response was simulated using initial conditions and the appropriate boundary conditions representing the experimental and geometrical constraints of the system. The simulation domain and the boundary conditions are illustrated in Figure 3. The

initial oxygen concentration within the domain of the simulation was set to 0.4 mM,[75] appropriate for aerated aqueous electrolyte solution at 5°C.

The boundaries shown in Figure 3 have the following conditions (n is the surface normal). Boundary 1 represents the axial symmetry in the cylindrical system, and so is set to have no normal oxygen flux ($\nabla c.n = 0$) at all times. Boundary 2 is the electrode, at which the oxygen concentration is zero because the electrode is held at a potential to reduce oxygen at a transport-limited rate (c = 0). Boundary 3 represents the substrate containing the chloroplast or thylakoid membrane films, so the flux of oxygen at this boundary is time and light dependent. In the dark, before the light is switched on, it is essentially inert, any consumption of oxygen due to respiration or other processes can be considered as negligible ($\nabla c.n = 0$). When the light is switched on, this boundary is governed by a rate law described in detail above. Boundaries 4 and 5 represent the surface of the glass surround of the electrode, and have no normal flux ($\nabla c.n = 0$). Boundary 6 and 7 represent the bulk solution, and are set to the bulk oxygen concentration (c = 0.4 mM).

As mentioned above the tip was held at a potential to detect oxygen naturally present in solution, before the light was switched on, and so the simulation evaluated this current which was allowed to reach steady-state, with no oxygen flux at the chloroplast or thylakoid membrane films. A typical example of the simulated oxygen concentration profile prior to illumination is illustrated in Figure 3 A, showing the profile characteristic of hindered diffusion. Upon illumination, an oxygen flux is applied at the substrate, which is ultimately manifested as a change in the tip current, from the reduction of oxygen, at the electrode. A typical simulated substrate boundary flux-time profile, from equation (3), with N_0 = 4.05 × 10^{-11} mol cm^{-2}, k_f = 0.17 s^{-1} and k_b = 0.03 s^{-1}, is shown in Figure 3 B. The corresponding tip current-time response is given in Figure 3 C; this highlights that the oxygen reduction current increases above the

background level (due to oxygen in the aerated solution), but quickly produces a peak followed by a decay to a steady response. The current at the electrode was determined from the integral of the normal flux of oxygen at the electrode surface multiplied by the Faraday constant and the number of electrons in the reduction of oxygen (which reasonably corresponds to 4).[76]

Results and Discussion

Chloroplast Intactness Measured Through Accessibility to Ferricyanide

The level of chloroplast intactness in a film of chloroplasts immobilized on PLL covered glass slides was determined by comparing the current responses for the oxidation of ferrocyanide at the tip, generated at the chloroplast film during illumination, before and after osmotically shocking the chloroplasts in the film. Figure 4 shows example current-time traces at a Pt SECM tip positioned 12.5 μm above a chloroplast film, for intact and osmotically shocked chloroplasts. The response upon illumination is fast, but finite, and is a combination of the response time of the photosynthetic system to illumination and the time taken for the ferrocyanide to diffuse from the substrate to the electrode, although the diffusion from the substrate to the electrode contributes most. The chloroplast envelope is known to be fairly impermeable to ferricyanide,[52] but once the envelope has been ruptured, through the osmotic shock, ferricyanide can freely diffuse to the thylakoid membrane and accept electrons at PSII.[53,55] The detection of ferrocyanide at the electrode demonstrates that the chloroplast envelope has been ruptured and that ferricyanide has been reduced at the illuminated thylakoid membrane.

The difference in the amount of ferrocyanide detected between the intact and osmotically shocked chloroplasts allows us to establish the percentage of intact chloroplasts in the initially immobilized film as ca. 75 %, by taking the ratio of current measured during illumination at intact and broken chloroplasts. It has been well documented that an average intactness of 70-80%

in solution is sufficient for studying photo-electron transport processes in chloroplasts and is typical for this method of chloroplast isolation.[48] Thus, the immobilization of the chloroplasts to a solid support results in minimal further rupture of the chloroplast envelope and allows the ready study of the photosynthetic pathway in this configuration.

Oxygen Evolution at Chloroplast Films

Oxygen evolution at chloroplast films, without any artificial electron acceptors in solution was detected at an electrode placed close to the films upon illumination. As highlighted earlier, oxygen evolution is the result of the photolysis of water occurring during the light reactions at PSII. Figure 5 A shows example current transients for diffusion-limited oxygen reduction at an Ag UME positioned 12.5 μm above a chloroplast film in isotonic HS buffer at four light intensities. As mentioned above, oxygen is detected at the SECM tip in the dark, as it is present naturally, and all currents are presented with respect to this value (I_{Dark}). For comparison Figure 5 B shows such an effect of the addition of $MgCl_2$, $MnCl_2$ and EDTA, present in the HS+ buffer, on the oxygen generation at chloroplast films.

Upon illumination of the immobilized chloroplast films, in both buffers, a sharp increase (spike) in oxygen flux at the electrode was observed. The appearance of an initial oxygen concentration spike has been reported previously, with Fork observing such a effect while investigating oxygen exchange at chloroplasts in solution in the absence of a Hill oxidant, using a macroscale Clark type oxygen electrode.[77] Matsue *et al.* also observed an initial intracellular oxygen spike in algal protoplasts using ultramicroelectrodes with ring radii of approximately 2 μm.[40,41] The oxygen spike was attributed to the consumption of the limited number of, then unknown, electron acceptors by Fork, and to the consumption of the limited number of terminal species (such as NADP) by Matsue. However, we observe an initial oxygen concentration spike

of the same magnitude over films of both chloroplasts and thylakoid membranes (discussed below), suggesting that the limiting factor responsible for the initial oxygen flux spike observed is not the terminal electron acceptors which are not present in the thylakoid membrane. Rather, it is more reasonably to propose a component of the linear electron transport pathway that is present in both systems, and we suggest that it is, in fact, the limited size, and regeneration, of the PQ pool for which we have developed the model above. This spike in oxygen concentration rapidly reached a peak and then decayed to a much lower steady-state net oxygen evolution rate which remained fairly constant for the remainder of the illumination period. Interestingly, a small oxygen consumption signal by the chloroplasts was observed when the light was turned off ($I_{Light} - I_{Dark}$ taking on negative values transiently). The oxygen consumption, after completion of the illumination period, is most likely the result of oxygen acting as an electron acceptor at PSI, upon depletion of the terminal electron acceptor, NADP, a process commonly referred to as the Mehler reaction.[1,2] Increasing light intensity resulted in the initial oxygen flux spike reaching larger current values, for example the maximum current increase from 30 pA to 190 pA in HS buffer (Figure 5 A) with an increase of light intensity from 16 % to 100 %. The quasi steady-state oxygen generation during illumination also showed a positive correlation with light intensity.

It is evident that the initial oxygen generation was much larger in the HS+ buffer compared to the HS buffer, with the lowest light fluxes (16 % and 26 %) showing a 5-6 times difference in the peak oxygen current. This is consistent with the enhanced photosynthetic activity that has been reported on bulk systems in the presence of the Mg^{2+} ions,[56,59,78] and could also be due to the presence of chloride ions or Mn^{2+} which play a crucial role in the water splitting complex.[57,79,80]

Using the FEM model described earlier, the rate of oxygen evolution over the initial forty seconds of illumination at the chloroplast film, for both HS and HS+ buffers, was calculated. The

first 40 seconds was chosen in order to incorporate the initial oxygen concentration spike and its subsequent decrease to a steady-state oxygen evolution current. The evolution of oxygen is based on the rate of consumption (k_f) and regeneration (k_b) of PQ, and the simulated response for the oxygen evolution in HS buffer is illustrated in Figure 5 C and D, alongside the corresponding experimental data. The rate constants (k_f, k_b and N_0), calculated by fitting the simulated response to the peak height, peak width at half height and quasi steady-state current, are summarized in Table 2. These results show a proportional relationship between k_f and light intensity. This was expected due to oxygen evolution being centered on a light driven process in photosynthesis. The initial oxygen generation strongly depends on the forward rate constant, k_f, but the longer time response has a weak dependence on the regeneration of the limited PQ pool, k_b. Interestingly, the total amount of PQ, N_0, which we calculated as part of the model was fairly consistent between the different simulations and in the different buffers.

We can compare the value of the total amount of PQ, N_0, to what we might expect within a chloroplast monolayer. We do so by using the ratio of the moles of chlorophyll to PQ in chloroplasts and from the ability to determine the surface coverage of the slides under the electrode area from the microscopy images. The amount of chlorophyll per chloroplast is *ca.* 1×10^{-15} moles,[81] and ratio of chlorophyll to PQ is *ca.* 70:1.[82] The optical microscope images, Figure 2 A, were used to calculate the number of chloroplasts per square centimeter (3.5×10^6) and hence the total number of moles of PQ per square centimeter was calculated by multiplying by the amount of chlorophyll per chloroplast and then dividing by the ratio of chlorophyll to PQ. The effective concentration of PQ, N_0, was *ca.* 5×10^{-11} mol cm^{-2}. This compares very well with the N_0 values calculated as part of the model. This further reinforces the idea that the PQ pool, and its state, has a massive influence on the oxygen generation profile during illumination.

Oxygen Evolution at Thylakoid Membrane Films

Local oxygen fluxes from films of immobilized thylakoid membranes in HM buffer were recorded under illumination. Although thylakoid membranes contain the light-driven components of photosynthesis they lack many other components of photosynthesis, most importantly the terminal electron acceptor, NADP. In the absence of an artificial electron acceptor, the oxygen fluxes generated by the thylakoid membranes, when illuminated, were found to be similar at very short times but different at long times, when compared to those measured from intact chloroplasts. This is evident in Figure 6, which shows the current measured at an Ag electrode placed above a film of thylakoid membranes, at a series of different light fluxes. An initial cathodic spike at the electrode, corresponding to oxygen generation, was observed upon illumination. This initial oxygen concentration spike increased with increasing light intensity, as found for the films of chloroplasts, except the peak at 100 % which was actually slightly lower than at 60 %. This is because the spike was followed by a rapid decrease of oxygen flux at the electrode to a level which indicated significant oxygen consumption by the thylakoid membranes under all light intensities. A steady-state current was obtained after approximately 60 seconds of illumination for this net oxygen consumption. The current measured at the tip, indicative of steady-state oxygen consumption, was found to increase with light intensity. Once the illumination period of 160 seconds was complete, and the light was switched off, the local oxygen flux at the electrode (tip current) returned to the dark steady-state current value.

It has been observed that during times of limited availability of electron acceptors for PSI, such as NADP, oxygen itself can act as the terminal electron acceptor (Mehler reaction).[1,2] The decrease in oxygen flux at thylakoid membranes, compared to chloroplasts, can be attributed, in part, to oxygen taking over as the main terminal electron acceptor and hence a competition is established between oxygen production and consumption. However, the steady-state oxygen

consumption indicates that additional light induced oxygen reduction is occurring at the thylakoid membranes.

The initial oxygen production rate was determined at each of the light intensities by analyzing the initial oxygen generation spike. The calculated initial fluxes and corresponding rate constants (fluxes divided by the average total amount of PQ, 4×10^{-11} mol cm^{-2}) are given in Table 3. The rate constants for oxygen generation show a reasonable trend, being proportional to the light flux. Moreover, as highlighted above, the rate constants for the generation of oxygen in thylakoid membrane films and the forward rate constant for chloroplasts films are broadly similar.

In past work, the initial oxygen concentration spike, which was observed with the chloroplast films (see above), has been ascribed to the rapid consumption of the limited number of terminal electron acceptors.[40,41] However, we have observed that the initial oxygen fluxes after illumination is of the same magnitude in both chloroplasts and thylakoid membranes. If the lack of terminal electron acceptors was responsible for controlling the oxygen generation rate, then one could reasonably have expected it to be significantly slower and less extensive in thylakoid membranes as compared to chloroplasts. Given our results, which have been obtained with much higher time resolution than in previous studies, it is perhaps more reasonable to consider the oxidation state of the PQ pool, and its size, to control the initial photo-generation of oxygen in both chloroplasts and thylakoid membranes.

Single Thylakoid Membrane Ferricyanide Reduction

We now turn to the case where we monitor photosynthetic activity via the artificial electron acceptor ferricyanide, which produces ferrocyanide[48–52] that is subsequently detected at the SECM tip. We investigate this process at the level of a single isolated thylakoid membrane using a 25 μm diameter Pt disk UME (as shown in Figure 2 C). Figure 7 shows typical current-time

responses for the detection of ferrocyanide for the following scenarios: (a) when the electrode was placed over an individual thylakoid membrane with no ferricyanide present; (b) at the same thylakoid membrane with 3.3 mM ferricyanide present; and, (c) in the bulk solution with no thylakoid membrane but with 3.3 mM ferricyanide. Without ferricyanide present, or with the tip in bulk solution, no significant change in current was detected upon illumination of the membrane. When ferricyanide was present and the tip was directly above a thylakoid membrane, an increase in the current was measured at the electrode during illumination, indicating that ferricyanide was reduced at the thylakoid membrane and detected as ferrocyanide at the electrode. The maximum current recorded corresponds to 1×10^{-16} mol s^{-1} of ferricyanide being reduced by a single thylakoid membrane. The proximity of the electrode to the thylakoid membrane and the size of the electrode with respect to the thylakoid membrane result in the detection of close to 100% of the ferrocyanide generated and so the current is a direct measurement of the thylakoid membrane activity. This corresponds, assuming a 2 μm radius thylakoid membrane, to a flux of 8×10^{-10} mol cm^{-2} s^{-1}, which is 200 times larger than the oxygen flux seen at the films of chloroplasts and thylakoid membranes.

Conclusions

SECM has been demonstrated to be a powerful method for the quantitative measurement of the local flux of redox active species from isolated chloroplasts and thylakoid membranes during photosynthesis. The ability to place an electrode precisely, within a few microns of the sample, has allowed effective, real-time measurements of redox processes not only from monolayer films of chloroplasts and thylakoid membranes, but also at single isolated thylakoid membranes. SECM has also been shown to provide an assay of chloroplast viability, demonstrating that chloroplasts deposited on PLL-modified substrates suffer from minimal ruptures, as determined

by the measurement of the oxidation of ferrocyanide before and after osmotically shocking chloroplast films.

Both oxygen generation and consumption has been determined directly at chloroplast and thylakoid membrane films under illumination. The chloroplast and thylakoid membrane films showed an initial oxygen generation flux which quickly peaks, with chloroplast films then reverting to steady-state oxygen production and thylakoid membrane films reverting to steady-state oxygen consumption at longer times. The trend in oxygen generation rate with time is most likely a result of the oxidation state of the limited PQ pool, and not, as previously reported, due to the limited availability of terminal electron acceptors.[40,41] The addition of $MgCl_2$, $MnCl_2$ and EDTA increases the generation of oxygen from chloroplast films, confirming that one, or more, of these components play a role in oxygen generation during photosynthesis. This aspect shows the possibility of using the SECM technique to study the role of various additives within photosynthesis.

Finite element modeling was used to quantify oxygen generation kinetics at the films. The model developed for the chloroplast films took account of the regeneration and consumption of available oxidized species and was used to rationalize the initial oxygen generation spike and subsequent oxygen generation. Fitting the model to the experimental data demonstrated that the rate constant for consumption of available PQ species, k_f, was significantly light dependent, while generation of the oxidized species, k_b, only showed a very weak dependence at higher light intensities. Further evidence for the validity of the model was that the PQ pool size estimated as a variable in the model compared well with values expected from literature. Furthermore, the initial oxygen generation rates for thylakoid membranes were consistent with those for chloroplasts, adding weight to the assumption that the PQ pool state, and size, controls the initial oxygen generation rates, rather than the presence of terminal electron acceptors.

Acknowledgments

We thank the EPSRC for studentships to K.M. (via the MOAC doctoral training centre) and S. M. We acknowledge support from a European Research Council Advanced Investigator Grant (ERC-2009-AdG247143 QUANTIF) for P.R.U. We are grateful to Prof. Julie Macpherson and Dr. Anna Whitworth for helpful comments and assistance in this work. Some of the equipment used was obtained through the Science City Advanced Materials project with support from Advantage West Midlands and the European Regional Development Fund.

References

(1) Hall, D. O.; Rao, K. K. *Photosynthesis*; Cambridge University Press, 1999.

(2) *Photosynthesis. A Comprehensive Treatise*; A. S. Raghavendra, Ed.; Cambridge University Press, 1998.

(3) Baker, N. R. Chlorophyll Fluorescence: A Probe of Photosynthesis In Vivo. *Annu. Rev. Plant Biol.* **2008**, *59*, 89–113.

(4) Izabela, R.; Katarzyna, G.; Borys, K.; Agnieszka, M. 3D Chloroplast Structure. In *Photosynthesis. Energy from the Sun: 14th International Congress on Photosynthesis*; Allen, J. F.; Grant, E.; Golbeck, J. H.; Osmond, B., Eds.; Springer, 2008; pp. 771–774.

(5) Vacha, F.; Bumba, L.; Kaftan, D.; Vacha, M. Microscopy and Single Molecule Detection in Photosynthesis. *Micron* **2005**, *36*, 483 – 502.

(6) Hall, D. O.; Edge, H.; Kalina, M. The Site of Ferricyanide Photoreduction in the Lamellae of Isolated Spinach Chloroplasts: A Cytochemical Study. *J. Cell Sci.* **1971**, *9*, 289–303.

(7) Jensen, R. G.; J. A. Bassham Photosynthesis by Isolated Chloroplasts. *Proc. Natl. Acad. Sci. USA* **1966**, *56*, 1095–1101.

(8) Shimoni, E.; Rav-Hon, O.; Ohad, I.; Brumfeld, V.; Reich, Z. Three-dimensional Organization of Higher-Plant Chloroplast Thylakoid Membranes Revealed by Electron Tomography. *Plant Cell* **2005**, *17*, 2580 – 2586.

(9) Kaftan, D.; Brumfeld, V.; Nevo, R.; Scherz, A.; Reich, Z. From Chloroplasts to Photosystems: in situ Scanning Force Microscopy on Intact Thylakoid Membranes. *EMBO J.* **2002**, *21*, 6146–6153.

(10) Sturgis, J. N.; Tucker, J. D.; Olsen, J. D.; Hunter, C. N.; Niederman, R. A. Atomic Force Microscopy Studies of Native Photosynthetic Membranes. *Biochemistry-US* **2009**, *48*, 3679–3698.

(11) Dahn, D. C.; Cake, K.; Hale, L. R. Scanning Tunneling Microscopy of Unbroken Chloroplasts. *Ultramicroscopy* **1992**, *42-44*, 1222 – 1227.

(12) Terai, T.; Nagano, T. Fluorescent Probes for Bioimaging Applications. *Curr. Opin. Chem. Biol.* **2008**, *12*, 515–521.

(13) Ntziachristos, V. Fluorescence Molecular Imaging. *Ann. Rev. Biomed. Eng.* **2006**, *8*, 1–33.

(14) Edwards, M. A.; Martin, S.; Whitworth, A. L.; Macpherson, J. V.; Unwin, P. R. Scanning Electrochemical Microscopy: Principles and Applications to Biophysical Systems. *Physiol. Meas.* **2006**, *27*, R63–R108.

(15) Sun, P.; Laforge, F. O.; Mirkin, M. V. Scanning Electrochemical Microscopy in the 21st Century. *Phys. Chem. Chem. Phys.* **2007**, *9*, 802–823.

(16) Amemiya, S.; Bard, A. J.; Fan, F.-R. F.; Mirkin, M. V.; Unwin, P. R. Scanning Electrochemical Microscopy. *Ann. Rev. Anal. Chem.* **2008**, *1*, 95–131.

(17) Schulte, A.; Nebel, M.; Schuhmann, W. Scanning Electrochemical Microscopy in Neuroscience. *Ann. Rev. Anal. Chem.* **2010**, *3*, 299–318.

(18) Mirkin, M. V.; Nogala, W.; Velmurugan, J.; Wang, Y. Scanning Electrochemical Microscopy in the 21st Century. Update 1: Five Years After. *Phys. Chem. Chem. Phys.* **2011**, *13*, 21196–21212.

(19) Bard, A. J.; Mirkin, M. V.; Unwin, P. R.; Wipf, D. O. Scanning Electrochemical Microscopy. 12. Theory and Experiment of the Feedback Mode with Finite Heterogeneous Electron-Transfer Kinetics and Arbitrary Substrate Size. *J. Phys. Chem.* **1992**, *96*, 1861–1868.

(20) Amphlett, J. L.; Denuault, G. Scanning Electrochemical Microscopy (SECM): An Investigation of the Effects of Tip Geometry on Amperometric Tip Response. *J. Phys. Chem. B* **1998**, *102*, 9946–9951.

(21) Cornut, R.; Griveau, S.; Lefrou, C. Accuracy Study on Fitting Procedure of Kinetics SECM Feedback Experiments. *J. Electroanal. Chem.* **2010**, *650*, 55–61.

(22) Kwak, J.; Bard, A. J. Scanning Electrochemical Microscopy. Theory of the Feedback Mode. *Anal. Chem.* **1989**, *61*, 1221–1227.

(23) Diakowski, P. M.; Ding, Z. Interrogation of Living Cells using Alternating Current Scanning Electrochemical Microscopy (AC-SECM). *Phys. Chem. Chem. Phys.* **2007**, *9*, 5966–5974.

(24) Takahashi, Y.; Miyamoto, T.; Shiku, H.; Ino, K.; Yasukawa, T.; Asano, R.; Kumagai, I.; Matsue, T. Electrochemical Detection of Receptor-mediated Endocytosis by Scanning Electrochemical Microscopy. *Phys. Chem. Chem. Phys.* **2011**, *13*, 16569–16573.

(25) Takahashi, Y.; Murakami, Y.; Nagamine, K.; Shiku, H.; Aoyagi, S.; Yasukawa, T.; Kanzaki, M.; Matsue, T. Topographic Imaging of Convoluted Surface of Live Cells by Scanning Ion Conductance Microscopy in a Standing Approach Mode. *Phys. Chem. Chem. Phys.* **2010**, *12*, 10012–10017.

(26) Beaulieu, I.; Kuss, S.; Mauzeroll, J.; Geissler, M. Biological Scanning Electrochemical Microscopy and Its Application to Live Cell Studies. *Anal. Chem.* **2011**, *83*, 1485–1492.

(27) Lee, C.; Kwak, J.; Bard, A. J. Application of Scanning Electrochemical Microscopy to Biological Samples. *Proc. Natl. Acad. Sci. USA* **1990**, *87*, 1740–1743.

(28) Schulte, A.; Schuhmann, W. Single-Cell Microelectrochemistry. *Angew. Chem. Int. Edit.* **2007**, *46*, 8760–8777.

(29) Bergner, S.; Wegener, J.; Matysik, F.-M. Simultaneous Imaging and Chemical Attack of a Single Living Cell within a Confluent Cell Monolayer by Means of Scanning Electrochemical Microscopy. *Anal. Chem.* **2011**, *83*, 169–174.

(30) Wang, Y.; Noël, J.-M.; Velmurugan, J.; Nogala, W.; Mirkin, M. V.; Lu, C.; Guille Collignon, M.; Lemaître, F.; Amatore, C. Nanoelectrodes for Determination of Reactive Oxygen and Nitrogen Species inside Murine Macrophages. *Proc. Natl. Acad. Sci. USA* **2012**, *109*, 11534–11539.

(31) Sun, P.; Laforge, F. O.; Abeyweera, T. P.; Rotenberg, S. A.; Carpino, J.; Mirkin, M. V. Nanoelectrochemistry of Mammalian Cells. *Proc. Natl. Acad. Sci. USA* **2008**, *105*, 443–448.

(32) Koley, D.; Bard, A. J. Inhibition of the MRP1-mediated Transport of the Menadione-glutathione Conjugate (Thiodione) in HeLa Cells as Studied by SECM. *Proc. Natl. Acad. Sci. USA* **2012**, *109*, 11522–11527.

(33) Koley, D.; Bard, A. J. Triton X-100 Concentration Effects on Membrane Permeability of a Single HeLa Cell by Scanning Electrochemical Microscopy (SECM). *Proc. Natl. Acad. Sci. USA* **2010**, *107*, 16783–16787.

(34) Kuss, S.; Cornut, R.; Beaulieu, I.; Mezour, M. A.; Annabi, B.; Mauzeroll, J. Assessing Multidrug Resistance Protein 1-mediated Function in Cancer Cell Multidrug Resistance by Scanning Electrochemical Microscopy and Flow Cytometry. *Bioelectrochem.* **2011**, *82*, 29–37.

(35) Longobardi, F.; Cosma, P.; Milano, F.; Agostiano, A.; Mauzeroll, J.; Bard, A. J. Scanning Electrochemical Microscopy of the Photosynthetic Reaction Center of Rhodobacter sphaeroides in Different Environmental Systems. *Anal. Chem.* **2006**, *78*, 5046–5051.

(36) Cai, C.; Liu, B.; Mirkin, M. V.; Frank, H. A.; Rusling, J. F. Scanning Electrochemical Microscopy of Living Cells. 3. Rhodobacter sphaeroides. *Anal. Chem.* **2002**, *74*, 114–119.

(37) Zhu, R.; Macfie, S. M.; Ding, Z. Effects of Cadmium on Photosynthetic Oxygen Evolution from Single Stomata in Brassica juncea (L.) Czern. *Langmuir* **2008**, *24*, 14261–14268.

(38) Tsionsky, M.; Cardon, Z. G.; Bard, A. J.; Jackson, R. B. Photosynthetic Electron Transport in Single Guard Cells as Measured By Scanning Electrochemical Microscopy. *Plant Physiol.* **1997**, *113*, 895–901.

(39) Yasukawa, T.; Kaya, T.; Matsue, T. Dual Imaging of Topography and Photosynthetic Activity of a Single Protoplast by Scanning Electrochemical Microscopy. *Anal. Chem.* **1999**, *71*, 4637–4641.

(40) Yasukawa, T.; Uchida, I.; Matsue, T. Microamperometric Measurements of Photosynthetic Activity in a Single Algal Protoplast. *Biophys. J.* **1999**, *76*, 1129–1135.

(41) Matsue, T.; Koike, S.; Abe, T.; Itabashi, T.; Uchida, I. An Ultramicroelectrode for Determination of Intracellular Oxygen. Light-irradiation-induced Change in Oxygen Concentration in an Algal Protoplast. *Biochim. Biophys. Acta* **1992**, *1101*, 69–72.

(42) Matsue, T.; Koike, S.; Uchida, I. Microamperometric Estimation of Photosynthesis Inhibition in a Single Algal Protoplast. *Biochem. Bioph. Res. Comm.* **1993**, *197*, 1283–1287.

(43) Faulkner, C. J.; Lees, S.; Ciesielski, P. N.; Cliffel, D. E.; Jennings, G. K. Rapid Assembly of Photosystem I Monolayers on Gold Electrodes. *Langmuir* **2008**, *24*, 8409–8412.

(44) Ciobanu, M.; Kincaid, H. A.; Jennings, G. K.; Cliffel, D. E. Photosystem I Patterning Imaged by Scanning Electrochemical Microscopy. *Langmuir* **2005**, *21*, 692–698.

(45) Fasching, R.; Ryu, W.-H.; Bai, S.-J.; Park, J.-S.; Fabian, T.; Moseley, J.; Grossman, A.; Prinz, F. AFM/EC Nano Probing of Single Cells and Organelles. *IEEE Sensors* **2007**, 699–702.

(46) Ryu, W.; Bai, S.-J.; Park, J. S.; Huang, Z.; Moseley, J.; Fabian, T.; Fasching, R. J.; Grossman, A. R.; Prinz, F. B. Direct Extraction of Photosynthetic Electrons from Single Algal Cells by Nanoprobing System. *Nano Lett.* **2010**, *10*, 1137–1143.

(47) Bai, S.-J.; Ryu, W.; Fasching, R. J.; Grossman, A. R.; Prinz, F. B. In Vivo O2 Measurement inside Single Photosynthetic Cells. *Biotechnol. Lett.* **2011**, *33*, 1675–1681.

(48) Hipkins, M. F. Introduction to Photosynthetic Energy Transduction. In *Photosynthesis energy transduction a practical approach*; Hipkins, M. F.; Baker, N. R., Eds.; IRL Press, 1986.

(49) Cerović, Z. G.; Plesnicar, M. An Improved Procedure for the Isolation of Intact Chloroplasts of High Photosynthetic Capacity. *Biochem. J.* **1984**, *223*, 543 – 545.

(50) Robinson, S. P.; Wiskich, J. T. Stimulation of Carbon Dioxide Fixation in Isolated Pea Chloroplasts by Catalytic Amounts of Adenine Nucleotides. *Plant Physiol.* **1976**, *58*, 156–162.

(51) Mourioux, G.; Douce, R. Slow Passive Diffusion of Orthophosphate between Intact Isolated Chloroplasts and Suspending Medium. *Plant Physiol.* **1981**, *67*, 470–473.

(52) Nakatani, H. Y.; Barber, J. An Improved Method for Isolating Chloroplasts Retaining their Outer Membranes. *Biochim. Biophys. Acta* **1977**, *461*, 510–512.

(53) Nicholls, D. G.; Ferguson, S. J. *Bioenergetics*; Academic Press, 2002.

(54) Barr, R.; Crane, F. L. Ferricyanide Reduction in Photosystem II of Spinach Chloroplasts. *Plant Physiol.* **1981**, *67*, 1190–1194.

(55) Banaszak, J.; Barr, R.; Crane, F. L. Evidence for Multiple Sites of Ferricyanide Reduction in Chloroplasts. *J. Bioenerg.* **1976**, *8*, 83–92.

(56) Shaul, O. Magnesium Transport and Function in Plants: The Tip of the Iceberg. *Biometals* **2002**, *15*, 309–323.

(57) Rivalta, I.; Amin, M.; Luber, S.; Vassiliev, S.; Pokhrel, R.; Umena, Y.; Kawakami, K.; Shen, J.; Kamiya, N.; Bruce, D.; Brudvig, G. W.; Gunner, M. R.; Batista, V. S. Structural-Functional Role of Chloride in Photosystem II. *Biochem* **2011**, *50*, 6312–6315.

(58) Critchley, C. The role of chloride in Photosystem II. *Biochim. Biophys. Acta* **1985**, *811*, 33–46.

(59) Pier, P. A.; Berkowitz, G. A. The Effects of Chloroplast Envelope-Mg(2+), Cation Movement, and Osmotic Stress on Photosynthesis. *Plant Sci.* **1989**, *64*, 45–53.

(60) Mills, W. R.; Joy, K. W. A Rapid Method for Isolation of Purified, Physiologically Active Chloroplasts, Used to Study the Intracellular Distribution of Amino Acids in Pea Leaves. *Planta* **1980**, *148*, 75–83.

(61) Arnon, D. I. Copper Enzymes in Isolated Chloroplasts. Polyphenoloxidase in Beta Vulgaris. *Plant Physiol.* **1949**, *24*, 1–15.

(62) Nugues, S.; Denuault, G. Scanning Electrochemical Microscopy: Amperometric Probing of Diffusional Ion Fluxes Through Porous Membranes and Human Dentine. *J. Electroanal. Chem.* **1996**, *408*, 125–140.

(63) Blizanac, B. B.; Ross, P. N.; Marković, N. M. Oxygen Reduction on Silver Low-Index Single-Crystal Surfaces in Alkaline Solution: Rotating Ring Disk(Ag(hkl)) Studies. *J Phys. Chem. B* **2006**, *110*, 4735–4741.

(64) James, S. D. The Electrochemical Activation of Platinum Electrodes. *J. Electrochem. Soc.* **1967**, *114*, 1113–1119.

(65) McGeouch, C.-A.; Peruffo, M.; Edwards, M. A.; Bindley, L. A.; Lazenby, R. A.; Mbogoro, M. M.; McKelvey, K.; Unwin, P. R. Quantitative Localized Proton-Promoted Dissolution Kinetics of Calcite Using Scanning Electrochemical Microscopy (SECM). *J. Phys. Chem. C* **2012**, *116*, 14892–14899.

(66) Lilley, R. M.; Fitzgerald, M. P.; Rienits, K. G.; Walker, D. A. Criteria of Intactness and the Photosynthetic Activity of Spinach Chloroplast Preparations. *New Phytol.* **1975**, *75*, 1–10.

(67) Aro, E. M.; Virgin, I.; Andersson, B. Photoinhibition of Photosystem II. Inactivation, protein damage and turnover. *Biochim. Biophys. Acta* **1993**, *1143*, 113–134.

(68) Müh, F.; Glöckner, C.; Hellmich, J.; Zouni, A. Light-induced Quinone Reduction in Photosystem II. *Biochim. Biophys. Acta* **2012**, *1817*, 44–65.

(69) Vass, I. Molecular Mechanisms of Photodamage in the Photosystem II Complex. *Biochim. Biophys. Acta* **2012**, *1817*, 209–217.

(70) Frigerio, S.; Campoli, C.; Zorzan, S.; Fantoni, L. I.; Crosatti, C.; Drepper, F.; Haehnel, W.; Cattivelli, L.; Morosinotto, T.; Bassi, R. Photosynthetic Antenna Size in Higher Plants Is Controlled by the Plastoquinone Redox State at the Post-transcriptional Rather than Transcriptional Level. *J. Biol. Chem.* **2007**, *282*, 29457–29469.

(71) Joliot, P.; Johnson, G. N. Regulation of Cyclic and Linear Electron Flow in Higher Plants. *Proc. Natl. Acad. Sci. USA* **2011**, *108*, 13317–13322.

(72) Kruk, J.; Strzałka, K. Dark Reoxidation of the Plastoquinone-pool is Mediated by the Low-potential Form of Cytochrome b-559 in Spinach Thylakoids. *Photosynth. Res.* **1999**, *62*, 273–279.

(73) Kruk, J.; Karpinski, S. An HPLC-based Method of Estimation of the Total Redox State of Plastoquinone in Chloroplasts, the Size of the Photochemically Active Plastoquinone-pool and its Redox State in Thylakoids of Arabidopsis. *Biochim. Biophys. Acta* **2006**, *1757*, 1669–1675.

(74) Rochaix, J.-D. Regulation of Photosynthetic Electron Transport. *Biochim. Biophys. Acta* **2011**, *1807*, 375–383.

(75) *CRC Handbook of Chemistry and Physics*; Lide, D. R., Ed.; 90th Editi.; CRC Press/Taylor and Francis: Boca Raton, FL, 2009.

(76) Gonsalves, M.; Barker, A. L.; Macpherson, J. V.; Unwin, P. R.; O'Hare, D.; Winlove, C. P. Scanning Electrochemical Microscopy as a Local Probe of Oxygen Permeability in Cartilage. *Biophys. J.* **2000**, *78*, 1578–1588.

(77) Fork, D. C. Action Spectra of O2 Evolution by Chloroplasts with & without Added Substrate, for Regeneration of O2 Evolving Ability by Far-red, & for O2 Uptake. *Plant Physiol.* **1963**, *38*, 323–332.

(78) Liang, C.; Xiao, W.; Hao, H.; Xiaoqing, L.; Chao, L.; Lei, Z.; Fashui, H. Effects of Mg(2+) on Spectral Characteristics and Photosynthetic Functions of Spinach Photosystem II. *Spectrochim. Acta A* **2009**, *72*, 343–347.

(79) Olesen, K.; Andréasson, L.-E. The Function of the Chloride Ion in Photosynthetic Oxygen Evolution. *Biochemistry-US* **2003**, *42*, 2025–2035.

(80) Popelková, H.; Yocum, C. F. Current Status of the Role of Cl(-) Ion in the Oxygen-evolving Complex. *Photosynth. Res.* **2007**, *93*, 111–121.

(81) D. W. Lawler *Photosynthesis: Molecular, Physiological and Environmental Processes*; 2nd ed.; Longman Scientific & Technical, 1993.

(82) McCauley, S. W.; Melis, A. Quantitation of Plastoquinone Photoreduction in Spinach Chloroplasts. *Photosynth. Res.* **1986**, *8*, 3–16.

Table 1. Composition of buffers; KOH was also added to all buffers to adjust the pH to 8.0.

Buffer	HEPES / mM	Sorbitol / M	ethylenediaminetetraacetic acid (EDTA) / mM	$MgCl_2$ / mM	$MnCl_2$ / mM
HS	50	0.33	-	-	-
2×HS	100	0.66	-	-	-
5×HS	250	1.65	-	-	-
HS+	50	0.33	2	1	1
HM	10	-	-	5	-

Table 2. Oxygen evolution rates of chloroplast films, in HS and HS+ buffers, calculated from fitting the finite element model to the experimental data.

Buffer	**Light Intensity**	N_o **/ mol cm^{-2} (± 0.1 × 10^{-11})**	k_f **/ s^{-1} (± 0.01)**	k_b **/ s^{-1} (± 0.01)**
HS	100%	3.4×10^{-11}	0.35	0.04
HS	60%	3.1×10^{-11}	0.13	0.02
HS	26%	3.5×10^{-11}	0.05	0.02
HS	16%	3.2×10^{-11}	0.03	0.03
HS+	100%	5.7×10^{-11}	1.17	0.01
HS+	60%	5.0×10^{-11}	0.75	0.01
HS+	26%	4.2×10^{-11}	0.39	0.01
HS+	16%	3.2×10^{-11}	0.28	0.01

Table 3. Oxygen evolution rates for the initial 1 second of oxygen generation of thylakoid membrane films calculated by fitting the finite element model to experimental data.

Buffer	**Light Intensity**	**Oxygen flux / mol cm^{-2} s^{-1} ($\pm$ 0.1 × 10^{-12})**	**Oxygen evolution initial rate constant (k/N_0) / s^{-1} ($\pm$ 0.01)**
HM	100%	3.9 × 10^{-12}	0.10
HM	60%	4.3 × 10^{-12}	0.11
HM	26%	2.8 × 10^{-12}	0.07
HM	16%	1.8 × 10^{-12}	0.04

Figure Captions

Figure 1. A) A simplified diagram of the light dependent components of photosynthesis imbedded within the thylakoid membrane, contained in the chloroplast, which is located within plant cells in higher plants. [1,2] The primary components of the photosynthetic pathway consist of photosystem II (PSII), cytochrome b_6f complex (cyt b_6f), photosystem I (PSI) and ATP synthase. PSII uses the energy from absorbed photons to split water. The electrons generated are transferred to cyt b_6f by plastoquinone (PQ), while also pumping protons across the membrane, and on to PSI by plastocyanin (Pc). PSI, though intermediary proteins, uses this and energy from absorbed photons to convert NADP to NADPH. ATP synthase uses the generated proton gradient to convert ADP to ATP. B) Schematic of the generation of ferrocyanide (from ferricyanide present in bulk) at a substrate film and its collection at the electrode tip.

Figure 2. A) Optical (left) and z-stack confocal (right) images of chloroplast films. B) Optical (left) and z-stack confocal (right) images of thylakoid membrane films. Scale bar is 50 μm on the optical images (left of A and B) and 2 μm on the confocal microscopy images (right of A and B). C) A single thylakoid membrane seen as the bright green spot in the middle of the image, with a 25 μm diameter Pt disk electrode, seen as the dark halo around the thylakoid membrane, placed 12.5 μm above (see text). Scale bar 25 μm.

Figure 3. A) The geometry and boundary conditions of the finite element model, not to scale, of a 25 μm diameter disk electrode situated 12.5 μm above an active surface. Axial symmetry reduces the problem to a two dimensional domain. Boundary 1 is the axis of symmetry, boundary

2 is the electrode, boundary 3 is the chloroplast or thylakoid membrane film, boundaries 4 and 5 are the glass surrounds of electrode and boundaries 6 and 7 are the bulk solution. The color map shows the steady-state oxygen concentration profile in the dark due to the reduction of oxygen at the tip. B) Typical oxygen flux at the chloroplast or thylakoid membrane film (boundary 3) applied as part of the FEM simulation. C) Typical oxygen reduction current magnitude at the electrode (boundary 2) calculated from the FEM simulation.

Figure 4. Light induced current magnitude for the oxidation of ferrocyanide at a 25 μm diameter Pt disk electrode, held at 0.2 V and 12.5 μm above a film of isolated chloroplasts, in an HS buffer (50 mM HEPES and 0.33 M Sorbitol) containing 1 mM ferricyanide, prior to, and after, osmotically shocking the chloroplasts. ↑ represents light on and ↓ represents light off.

Figure 5. Current-time responses, that have been background (dark) current (4.0 ± 0.3 nA) subtracted, at a 25 μm diameter Ag disk electrode held at -0.9 V and 12.5 μm above a chloroplast film on a PLL-covered substrate for the reduction of oxygen as the sample was illuminated at four different light intensities (100%, 60%, 26% and 16%) in A) HS buffer (50 mM HEPES and 0.33 M Sorbitol) and B) in HS+ buffer (50 mM HEPES, 0.33 M Sorbitol, 2 mM EDTA, 1 mM $MgCl_2$ and 1 mM $MnCl_2$). C) and D) Experimental data for the oxygen reduction at the chloroplast film in HS and HS+ buffers, respectively, fitted to the FEM model using the parameters in Table 2. ↑ represents light on and ↓ represents light off.

Figure 6. Current responses, that have been background (dark) current (4.0 ± 0.3 nA) subtracted, for the reduction of oxygen at a 25 μm diameter Ag disk UME held at -0.9 V and 12.5 μm above a thylakoid membrane film on a PLL-covered substrate in HM buffer (10 mM HEPES and 5 mM $MgCl_2$) at a series of light intensities. ↑ represents light on and ↓ represents light off.

Figure 7. Current-time curves for the oxidation of ferrocyanide in HM buffer (10 mM HEPES and 5 mM $MgCl_2$) at a 25 μm diameter Pt disk electrode held at 0.2 V and 12.5 μm above a single thylakoid membrane during illumination for 30 seconds, in the absence (blue) and presence (red) of 3.3 mM ferricyanide; and in bulk solution with 3.3 mM ferricyanide (green).

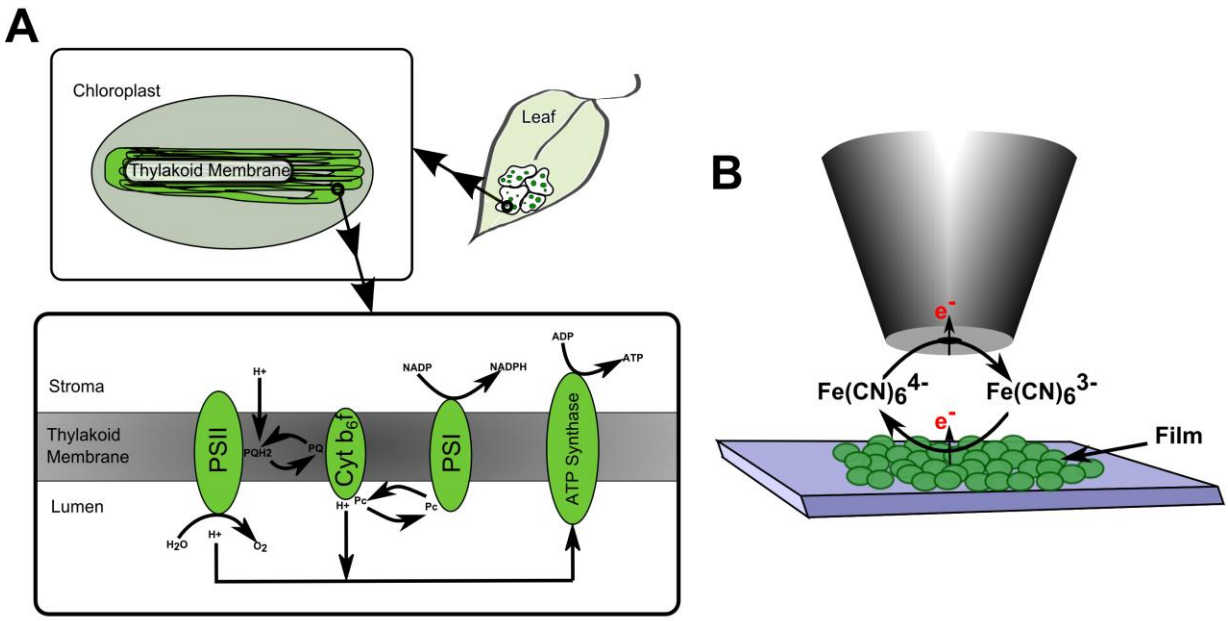
A
Chloroplast
Thylakoid Membrane
Leaf
Stroma
Thylakoid Membrane
Lumen
H+
PQH2
PQ
PSII
Cyt b6f
PSI
ATP Synthase
NADP
NADPH
ADP
ATP
H2O
O2
Pc
B
e-
Fe(CN)6 4-
Fe(CN)6 3-
Film

Figure1

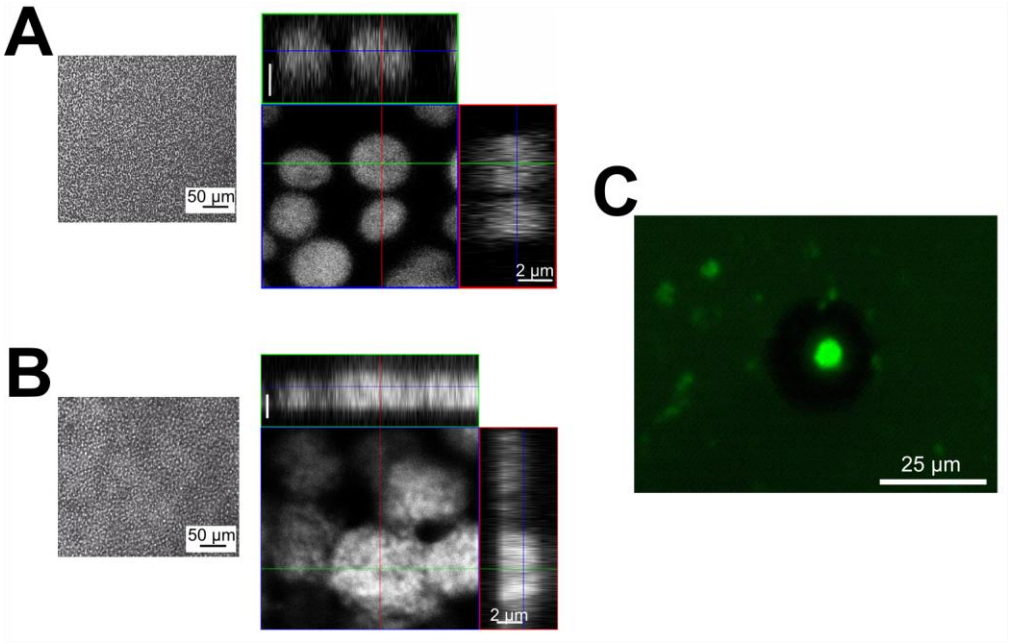

Figure 2

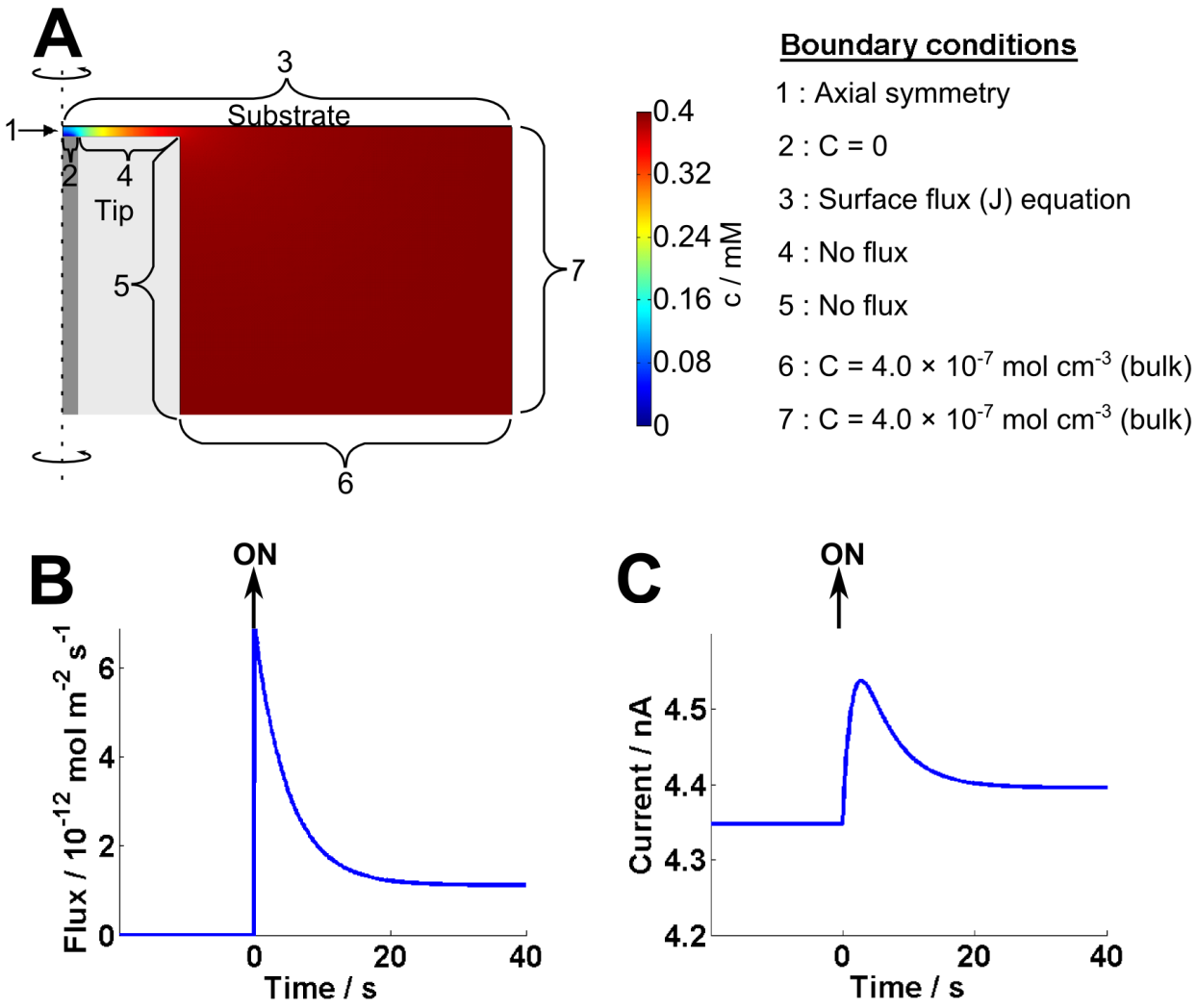
A
3
Substrate
1
2
4
Tip
5
7
6
0.4
0.32
0.24
0.16
0.08
0
c / mM
Boundary conditions
1 : Axial symmetry
2 : C = 0
3 : Surface flux (J) equation
4 : No flux
5 : No flux
6 : C = 4.0 × 10-7 mol cm-3 (bulk)
7 : C = 4.0 × 10-7 mol cm-3 (bulk)
B
ON
Flux / 10-12 mol m-2 s-1
0
2
4
6
0
20
40
Time / s
C
ON
Current / nA
4.2
4.3
4.4
4.5
0
20
40
Time / s

Figure 3

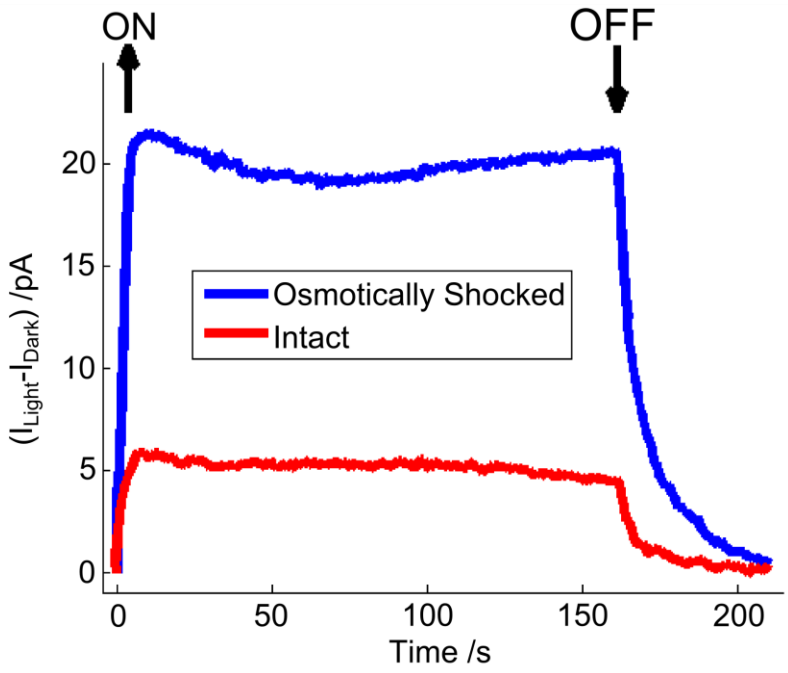
ON
OFF
20
15
10
5
0
(I_Light-I_Dark) /pA
Osmotically Shocked
Intact
0
50
100
150
200
Time /s

Figure 4

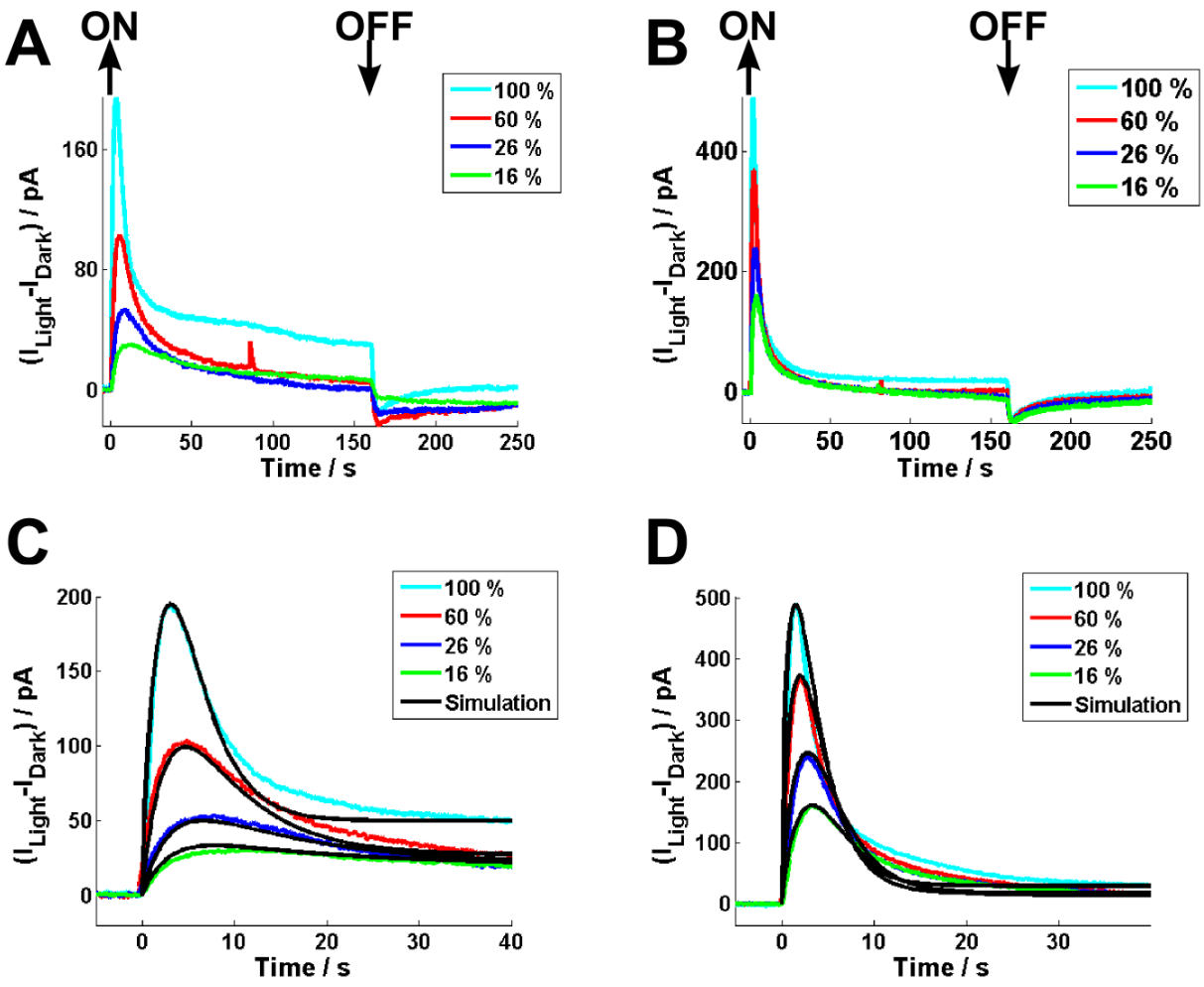
A
ON
OFF
100 %
60 %
26 %
16 %
(I_Light-I_Dark) / pA
Time / s
B
ON
OFF
100 %
60 %
26 %
16 %
(I_Light-I_Dark) / pA
Time / s
C
100 %
60 %
26 %
16 %
Simulation
(I_Light-I_Dark) / pA
Time / s
D
100 %
60 %
26 %
16 %
Simulation
(I_Light-I_Dark) / pA
Time / s

Figure 5

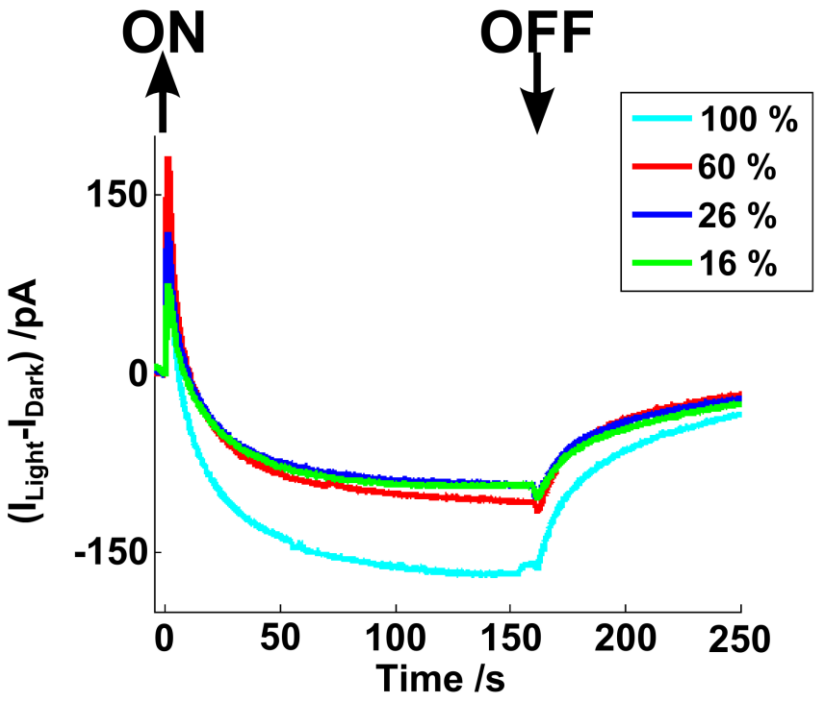
ON
OFF
100 %
60 %
26 %
16 %
150
0
-150
(I_Light-I_Dark) /pA
0
50
100
150
200
250
Time /s

Figure 6

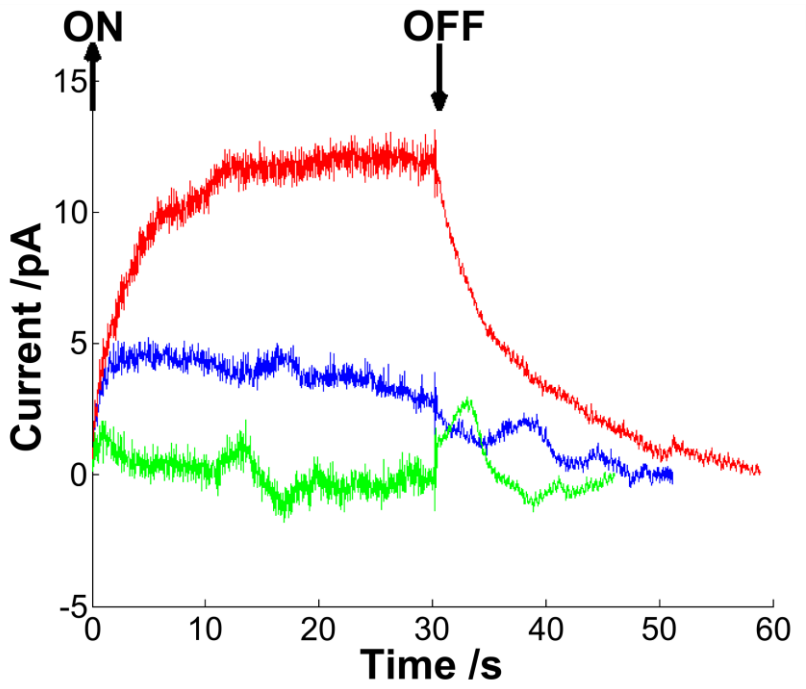

Figure 7

TOC